Effects of Air-Based Nonequilibrium Atmospheric Pressure Plasma Jet Treatment on Characteristics of Polypropylene Film Surfaces

Retsuo Kawakami,[*,1] Yuki Yoshitani,[1] Kimiaki Mitani,[1] Masahito Niibe,[2] Yoshitaka Nakano,[3] Chisato Azuma[1] and Takashi Mukai[4]

[1] *Graduate School of Science and Technology, Tokushima University, Tokushima 770-8506, Japan*

[2] *Laboratory of Advanced Science and Technology for Industry, University of Hyogo, Kamigori, Hyogo 678-1205, Japan*

[3] *Chubu University, Kasugai, Aichi 487-8501, Japan*

[4] *Nichia Corporation, Anan, Tokushima 774-0044, Japan*

* Corresponding author. E-mail: retsuo@ee.tokushima-u.ac.jp, Phone: +81 88 656 7441, Fax: +81 88 656 7441

Abstract

Polypropylene (PP) film surfaces were treated using air-based nonequilibrium atmospheric pressure plasma jets generated with a twisted wires-cylindrical electrode configuration. For comparison, PP samples were also processed with Ar plasma jets. The flux of charged particles imparted to the polymer surface by the air plasma jet greatly increased with decreases in both the gas flow rate and nozzle-to-sample distance, which was not the case for the Ar plasma jet. Reducing the gas flow rate and the nozzle-to-sample distance greatly enhanced the extent to which the surface was rendered hydrophilic by the air plasma within a short treatment time of 1 min. This enhanced effect is believed to originate from a high concentration of oxygen-based functional polar groups (FPGs) containing C−O/C−OH and C=O/C=O−OH bonds grafted onto the surface. The hydrophilic surfaces resulting from this process also exhibited nanopore structures. The large number of oxygen-based FPGs produced by the air plasma can be attributed primarily to oxygen radical ions impinging from the air plasma on the surface. This can further be attributed secondarily to heat-induced oxidation rather than the sticking of oxygen radicals and UV-induced oxidation from the plasma. The nanoporous structure can also be ascribed to oxidation from UV photogenerated holes.

Keywords: air plasma jet, polypropylene film, oxygen radical ions, heat-induced oxidation, oxygen radicals, ultraviolet-induced oxidation

1. Introduction

Polypropylene (PP) is a polyolefin thermoplastic polymer composed of CH_2=CH–CH_3 repeating units. PP and related materials are widely used for applications in various fields within the electrical, automotive, and chemical industries [1–3]. Some examples of these applications include lithium ion battery separators [1], automotive bodies [2] and packaging films [3]. PP-related materials can exhibit exceptional properties and have been widely researched [4–10] as a result of various advantages, such as low cost, easy processing, mechanical toughness, high chemical resistance, and high electrical resistivity [11-15]. However, PP also has various disadvantages, including poor wettability and inferior adhesive properties, which limit biomedical and biological applications. These disadvantages originate from a lack of functional polar groups (FPGs) containing O and N, such as carbonyl and amide moieties [16,17]. Grafting stable FPGs onto the PP surface would therefore impart improved wettability and adhesive properties.

Treatment using a nonequilibrium atmospheric pressure (AP) plasma jet is currently the most promising technique for generating FPGs on polymer surfaces [18−21]. This process can effectively modify the surface properties of the polymer without affecting the bulk characteristics of the material. This treatment is also extremely attractive because an AP plasma is readily generated without the vacuum components required to produce a nonequilibrium low pressure plasma [22,23]. In addition, an AP plasma jet induces minimal surface damage because it involves lower energy charged particles [24,25].

There have been numerous reports concerning the modification of PP film surfaces using nonequilibrium AP plasma jets [26−29]. As an example, Chen *et al*. treated PP film surfaces for 5 min using an Ar/O_2 plasma jet [30] and found that the contact angle of the surface decreased from 100° to 20°. However, such long treatment times can be

problematic with regard to industrial applications. The same group also treated PP film surfaces for 1 min with an Ar/O_2 plasma in conjunction with an allylamine ($C_3H_5NH_2$) monomer that contributed to the generation of enhanced hydrophilicity [30]. This modification decreased the contact angle to 20°, although the use of an allylamine monomer is undesirable in terms of cost and convenience.

A further advantage of air-based nonequilibrium AP plasma treatment is the use of the ambient atmosphere as the discharge gas, and there have been many reports concerning the modification of PP film surfaces with air plasma jets [31,32]. Akishev *et al*. treated PP film surfaces with an air plasma jet generated using a pins-to-plate discharge electrode configuration [31]. This apparatus comprised a single row of seven pins grounded electrically and an anode plate powered by a direct high voltage current. A flow of air was produced by a fan and directed perpendicular to the discharge current. Jacobs *et al*. upgraded the pins-to-plate discharge electrode configuration for industrial applications and demonstrated the in-line processing of PP films with samples mounted on a rotating drum [32]. However, the air plasma jet generated in this device did not greatly decrease the contact angle of PP film surfaces compared with the results obtained using an Ar/O_2 plasma jet [30−32]. A more detailed understanding of the interactions between PP film surfaces and particles/photons from the air plasma jet is therefore required to further improve the poor wettability and adhesive properties of PP films.

In the present study, we investigated the effects of the air-based nonequilibrium AP plasma jet treatment of PP film surfaces, employing a new plasma jet device having a twisted wires-cylindrical electrode configuration. This apparatus was developed by the authors specifically to generate an air-based nonequilibrium AP plasma jet for the present study, and differs from those previously reported in the literature [31,32]. For the sake of comparison, PP film surfaces were also treated with an Ar nonequilibrium

AP plasma jet generated using the same electrode configuration. In these trials, the air jet was supplied by an air compressor while the Ar jet was supplied by a high pressure gas cylinder. The twisted wires were powered by a high voltage bipolar impulse supply and the same voltages were applied to the air and Ar plasma jets. The present study focused primarily on variations in the wettability, chemical composition and morphology of the plasma-treated PP film surfaces. These changes in the PP film surfaces were investigated while changing the air flow rate, the distance from the jet nozzle to the PP film surface, and the plasma treatment time. Differences in the characteristics of the PP film surfaces treated with the air and Ar plasma jets were also assessed. Herein, we discuss and characterize the effects of air plasma jet treatment in terms of the impacts of oxygen radicals, ultraviolet (UV) radiation and heat imparted by the plasma. The present study emphasizes that the air plasma jet treatment of PP film surfaces performed in conjunction with the newly-designed twisted wires-cylindrical electrode configuration is a viable means of enhancing wettability and is competitive with other plasma jet treatments.

2. Material and methods

The air plasma jet treatment of PP film surfaces was carried out employing the plasma jet device shown in Fig. 1, which also provides a bottom view of the discharge tube. This apparatus incorporated three differently shaped electrodes, having wire, cylindrical and plate morphologies. The wire electrode was prepared by twisting four tungsten wires, each 0.5 mm in diameter. This was necessary because, in the case that the four wires were not twisted, the air plasma was not emitted from the nozzle in the form of a jet. We suspect that a turbulent flow was induced by twisting the four wires, but elucidating the details of the mechanisms by which the air plasma jet or the air plasma plume were generated will require systematic investigations based on changing

the number of twisted wires. The wire electrode was placed in a glass tube with an inner diameter of 3 mm and an outer diameter of 6 mm, such that the front edge of the electrode was located 1 mm from the jet nozzle. The cylindrical electrode was made of copper and was 50 mm in length and 0.1 mm in thickness. This electrode was positioned outside the glass tube 10 mm from the jet nozzle and was electrically grounded. The plate electrode was made of stainless steel and served as the sample stage. This electrode was covered with a 2 mm thick layer of glass and was electrically grounded. The distance from the jet nozzle to the sample stage or the sample surface was varied from 1 to 5 mm. The air flow consisted of ambient air provided by a compressor and the room temperature and relative humidity (RH) were 24 °C and 35%−40% RH, respectively. The air flow rate was varied from 3 to 10 l/min to produce the plasma jet shown in Fig. 2(b). The length of the plasma plume was observed to increase from approximately 5 to 8 mm as the air flow was increased. For comparison purposes, an Ar plasma jet was also generated, as shown in Fig. 2(c), using 99.9 vol% purity Ar supplied from a high pressure gas cylinder. The Ar flow rate was varied over the same range as the air flow rate, although the length of the Ar plasma plume remained relatively constant with increases in flow rate, at approximately 25 mm.

The wire electrode was powered by a 100 kHz bipolar impulse waveform generator with a repetition frequency of 10 kHz (Tamaoki Electronics TE-HVP1010K300-NP), as shown in Fig. 3(a). The voltage waveform was monitored using an oscilloscope (Agilent DSO1024A) equipped with a high-voltage probe (Agilent N2771A). The maximum and minimum values of the impulse voltage applied to the electrode were 7 and −10 kV, respectively, and the root mean square (RMS) value of the applied impulse voltage was 2.7 kV. The waveforms of the discharge currents flowing into the cylindrical electrode and the sample stage, I_C and I_S, were monitored through 10 Ω resistors, using the same oscilloscope as employed in the high voltage measurements, as shown in Figs.

3(b)−3(e). There were numerous filaments in the current waveforms of I_C and I_S for 3 and 10 l/min air plasma jets. The number of filaments with high currents for 3 l/min air plasma jet was seen to be larger. A detailed comparison between the discharge currents is shown in Fig. 4. The RMS values of I_C and I_S in Fig. 4 were estimated from the current waveforms based on the square root of the mean square of the current waveform over a single cycle. This estimation was performed five times and the estimated values were obtained by averaging the resulting data. In the case of the air plasma jet, the RMS value of I_C decreased from 220 to 200 mA as the gas flow rate increased from 3 to 10 l/min (see Fig. 4(a)) regardless of the nozzle-to-sample distance. An increase in the air flow will suppress increases in the temperature of the electrode, and so reduce increases in the gas temperature [33]. This effect, in turn, lowers the density of the air plasma generated by interactions between electrons and gas molecules, thus decreasing the RMS value of I_C. This is based on the fact that increasing the gas temperature increases the kinetic energy of gas molecules, which activates ionization of gas molecules and increases the plasma density [34,35]. In contrast, the RMS value of I_S was smaller than that of I_C and decreased as the nozzle-to-sample distance increased from 1 to 5 mm (see Fig. 4(b)). At a nozzle-to-sample distance of 1 mm, the RMS value of I_S greatly decreased, from 100 to 75 mA, as the gas flow rate increased, for the same reasons as provided above to explain the change in I_C. Conversely, the RMS value of I_S at a nozzle-to-sample distance of 3 mm was slightly decreased by increasing the gas flow rate, while the RMS value of I_S at a nozzle-to-sample distance of 5 mm was only minimally decreased upon increasing the gas flow rate. In the case of the Ar plasma jet, the RMS values of I_C and I_S were similar, as shown in Figs. 4(c) and 4(d), and were both smaller than those obtained using the air plasma jet. In addition, the RMS value of I_C changed very little as the gas flow rate and the nozzle-to-sample distance were increased, while the RMS value of I_S did not depend on the nozzle-to-sample distance

but decreased as the gas flow rate increased. Comparing the RMS values of I_S associated with the air and Ar plasma jets suggests that the flux of charged particles in the air plasma jet impinging on the sample surface greatly increased with decreases in both the gas flow rate and nozzle-to-sample distance. This change was much greater than that observed when using the Ar plasma jet.

Figure 5 demonstrates that the air and Ar plasma jets generated different emission spectra, based on data acquired using a spectrometer (Ocean optics USB4000) over the wavelength range of 200–900 nm with a resolution of 0.225 nm. These emission spectra were collected using an optical fiber 0.6 mm in diameter, placed 1 mm from the jet nozzle. The exposure time was 3 s. The emission spectrum generated by the air plasma jet contained peaks in the UV region between 300 and 400 nm and in the visible region between 750 and 800 nm. The peaks in the UV region are attributed to the emission of the N_2 second positive system, involving transitions from the upper $C^3\Pi_u$ state to the lower $B^3\Pi_g$ state, 2P(v",v'), where v" and v' are the vibrational quantum numbers of the upper and lower states, respectively [36−38]. Specifically, the peaks at UV wavelengths of 298, 316, 337, 358 and 380 nm (corresponding to photon energies of 3.2–4.2 eV) correspond to 2P(2,0), 2P(1,0), 2P(0,0), 2P(0,1) and 2P(0,2) transitions, respectively. The majority of the peaks observed in the visible region are attributed to the emission of the N_2 first positive system, involving transitions from the upper $B^3\Pi_g$ state to the lower $A^3\sum_u^+$ state, 1P(v",v') [36,39,40]. The remaining peak in the visible region, at 777 nm, is ascribed to emissions from excited oxygen atoms or radicals, OI [41,42]. In contrast, the emission spectrum of the Ar plasma jet was observed to contain no peaks in the UV region and peaks only in the visible range from 700 to 800 nm. The most intense peaks resulted from the emission of excited Ar atoms, ArI [42], while the other, less intense peak is attributed to emissions from excited oxygen atoms or radicals, OI [42]. These results were not changed while varying the gas flow rate. Magnifying the Ar plasma

spectrum in the UV region does show some peaks (see the inset to Fig. 5(b)) that are consistent with those reported in the literature [43,44] but much less intense. This discrepancy may be related to the turbulent flow induced by twisting the four wires, but the cause will need to be investigated in more detail in future work. However, the intensity of light emitted from the Ar plasma jet was larger than that of light emitted from the air plasma jet, as shown in Fig. 5. Specifically, the intensities of UV and OI peaks emitted from the Ar plasma jet were approximately 10 and 300 times larger, respectively.

The specimens used were PP monolayer films with a thickness of 80 μm and a melting point of 142 °C, supplied by the Toppan TDK Label Co., Ltd., Japan. These specimens were cut into small samples 10 × 10 mm^2 in size. Prior to the plasma jet treatments, the samples were ultrasonically cleaned in methanol, ethanol and deionized water for 15 min to remove contamination from the surfaces. Subsequently, the samples were dried with N_2 gas. These samples were subjected to plasma treatment times of 1, 2, 3 or 5 min. At a flow rate of 3 l/min and a nozzle-to-sample distance of 1 mm, a hole was burned through the sample when applying the air plasma jet for 5 min. For this reason, the wettability of this sample could not be assessed.

Changes in surface wettability were assessed by determining the static contact angles of 2 μl portions of deionized water dropped onto the surface, using a contact angle meter (Kyowa Interface Science CA-V200, Japan). The contact angle of the untreated PP film surface was 100°, indicating a hydrophobic surface. This measurement was performed three times for each plasma jet treatment and the three replicate values were averaged. Variations in the chemical composition of each plasma-treated surface were analyzed using X-ray photoelectron spectroscopy (XPS, Ulvac-Phi PHI500), based on assessing C 1s, O 1s and N 1s peaks with Al Kα radiation (1486.6 eV). Surface morphological changes were observed by scanning electron

microscopy (SEM, JEOL JSM-6390).

3. Results

3.1. Wettability changes

The air plasma treatment markedly affected the contact angle at the PP film surfaces, as is evident from Figs. 6(a)−6(c). Figure 6(a) plots the contact angle values as functions of treatment time for various flow rates at a nozzle-to-sample distance of 1 mm. The contact angle at zero treatment time corresponds to that of the untreated PP film surface. Interestingly, the change in the contact angle at a high flow rate of 10 l/min differs from that at lower rates of 3 and 5 l/min. The contact angle of the surface treated at a high flow rate decreased to 50° over a short treatment time of 1 min, but there were almost no further changes on increasing the treatment time from 1 to 5 min. The results obtained at the high rate were also constant even as the nozzle-to-sample distance was increased from 1 to 5 mm, as shown in Figs. 6(b) and 6(c). These results indicate that the plasma treatment with a high flow rate did not sufficiently enhance the PP surface hydrophilicity, regardless of the nozzle-to-sample distance.

In contrast, the contact angle of the surface treated using the low flow rates markedly decreased as the treatment time was prolonged, up to a specific time at which it plateaued. It is noteworthy that, at a low flow rate of 3 l/min, the contact angle drastically decreased to 20° over a short treatment time of 1 min. It is therefore evident that air plasma treatment in conjunction with a lower flow rate significantly enhances the hydrophilicity of the PP over a short treatment time. However, as demonstrated in Figs. 6(b) and 6(c), the contact angle did not decrease in the same manner over short treatment times as the nozzle-to-sample distance was increased. In particular, at a nozzle-to-sample distance of 5 mm, the contact angle did not become sufficiently small. These data suggest that an air plasma treatment employing a lower flow rate does not

enhance hydrophilicity as the nozzle-to-sample distance increases. The effects of both the nozzle-to-sample distance and the flow rate on contact angle are in agreement with the trends observed for the I_S RMS values. That is, the contact angle is correlated with the RMS value of I_S for the air plasma.

The contact angle results obtained using the Ar plasma greatly differed from those obtained with the air plasma, as shown in Fig. 6(d). When using the Ar plasma, the contact angle decreased to 48−58° over a short treatment time of 1 min regardless of changes in the gas flow rate and was only minimally affected by increases in treatment time. The same trend was also observed even at long nozzle-to-sample distances of 3 and 5 mm. Thus, the air plasma effectively enhanced the hydrophilicity of the PP at lower flow rates and nozzle-to-sample distances, while the Ar plasma behaved quite differently.

The contact angles of PP film surfaces treated using air plasma jets generated with the proposed twisted wires-cylindrical electrode configuration and with the pins-to-plate electrode configuration reported in the literature were compared [31,32]. The former configuration greatly decreased the contact angle, to 20°, while the latter configuration gave a higher value of 36° [31,32]. This contact angle obtained in the present study is equal to that obtained using an Ar/O_2 plasma jet as reported in the literature [30] and to that induced by an allylamine monomer-assisted Ar/O_2 plasma jet [30]. We also compared the treatment times required to produce a contact angle of 20° using the air plasma jet generated with the proposed electrode configuration to that reported for other plasma jets. We found that the required treatment time at a low gas flow rate of 3 l/min in the present study, 1 min, is shorter than the span of 5 min required for an Ar/O_2 plasma jet and comparable to that for an allylamine monomer–assisted Ar/O_2 plasma jet [30]. These comparisons indicate that air plasma jet treatment using a low flow rate together with the proposed twisted wires-cylindrical electrode configuration is an

effective means of enhancing the hydrophilicity of PP film surfaces over a short treatment time of 1 min.

3.2. Chemical composition changes

The air plasma treatment significantly modified the chemical compositions of the PP film surfaces as compared with the results obtained from the Ar plasma treatment (see Fig. 7). Figure 7(a) shows the C 1s region of the XPS spectrum for the untreated PP film surface, while Figs. 7(b) and 7(c) present the C 1s spectral regions for the surfaces treated for 1 min with air plasma jets at gas flow rates of 3 and 10 l/min and Fig. 7(d) provides the same data for a 3 l/min Ar plasma-treated surface. The samples subjected to the air plasma produced two peaks at binding energies of 285.0 and 289.3 eV regardless of the gas flow rate. In the case of Ar plasma treatment, a peak appeared at a binding energy of 285.0 eV, which was similar to that produced by the untreated PP film surface. The differences between the spectra can be emphasized by deconvolution of the spectra into three pseudo-Voigt functions: C1, C2 and C3. The C1 function is associated with C–C/C=C/C–H bonds at a binding energy of 285.0 eV [30,45,46]. The C2 function is attributed to C–O/C–OH bonds at a binding energy of 286.5 eV [45,46], while the C3 function is associated with C=O/C=O–OH bonds at a binding energy of 289.3 eV [45,46].

Figure 7(e) provides a detailed comparison of the chemical compositions of treated surfaces obtained from the peak deconvolution analysis. The untreated surface contained 1% oxygen-based FPGs with C−O/C−OH bonds. Following the air plasma treatment, the proportion of these FPGs increased, to 44% and 60%, as the gas flow rate decreased from 10 to 3 l/min. The 60% oxygen-based FPGs were composed of 40% C−O/C−OH bonds and 20% C=O/C=O−OH bonds. After the Ar plasma treatment, only 27% oxygen-based FPGs were grafted onto the surface. The 60% proportion of

oxygen-based FPGs obtained using the 3 l/min air plasma jet is high compared with reports in the literature [30]. In prior work, 40% FPGs composed of 25% oxygen species and 15% nitrogen species were grafted using an Ar/O_2 plasma jet with the assistance of an allylamine monomer. Thus, an air plasma jet treatment with a low gas flow rate is a more efficient approach to introducing high concentrations of oxygen-based FPGs in a short treatment time of 1 min.

The O 1s spectra of the air and Ar plasma-treated surfaces do not show two peaks but do exhibit chemical shifts to higher binding energies compared with the untreated PP film surface. The chemical shift values induced by the air and Ar plasma jets were approximately 1 and 0.2 eV, respectively. These data indicate that a larger number of O=C bonds that have a binding energy of 533.7 eV [47] were grafted by the air plasma jet, in addition to more O−C bonds associated with a binding energy of 532.4 eV [47], as compared with the Ar plasma jet. The O 1s peak deconvolution results in Figs. 8(a), 8(b) and 8(c) allow estimations of the proportions of O=C and O−C bonds in the treated surfaces (see Fig. 8(d)). The resulting ratios are consistent with those estimated from the C 1s peak data in Fig. 7(e). Only the Ar plasma-treated surface produced a N 1s peak. However, the ratio of the integrated intensities of the N 1s and C 1s peaks was determined to be 0.05, which is much smaller than the O 1s to C 1s ratio of 0.4. This finding suggests that neither the air nor the Ar plasma treatments grafted a large number of nitrogen species onto the surface.

3.3. Morphological changes

As demonstrated by Fig. 9, the air plasma treatment also more significantly changed the morphology of PP film surfaces as compared with the Ar plasma treatment. These morphological variations stem from the semi-crystalline nature of the polymer, which contained crystalline and amorphous lamellae [48]. In particular, portions of the

amorphous lamellae can be preferentially deformed by plasma jet irradiation. In the case of the 3 l/min air plasma jet, pronounced changes in surface morphology were evident following a treatment time of 60 s, as shown in Figs. 9(a)−9(d). The morphology of the surface treated for 2 s was similar to that of the untreated PP film surface, and this similarity suggests that the surface treated for 2 s was relatively smooth. At a plasma treatment time of 15 s, a large number of grain-like structures were formed together with a smaller quantity of stripe-like structures on the treated surface. These morphologies are likely related to the lamellar structure [48]. Upon extending the plasma treatment time to 30 s, a greater number of stripe-like structures were clearly observed to grow and, after 60 s, numerous nanopores with diameters less than 1 μm were produced along a striped pattern. Thus, the air plasma treatment with a low gas flow rate generated grainy, striped surface textures while forming nanopores as the treatment time was lengthened.

In the case of the 10 l/min air plasma jet, a different trend was observed with regard to the surface morphological changes (see Figs. 9(e)−9(h)). Here, the morphology of the surface treated for 2 s was similar to that of the untreated PP film surface, as was also observed following treatment with the 3 l/min air plasma jet. After processing for 15 s, grainy and striped structures were formed on the surface, similar to those induced by the 3 l/min air plasma jet treatment after 30 s. These same mixed structures were also obtained after lengthening the treatment time to 60 s. This result indicates that the air plasma treatment in conjunction with high flow rates induces grainy, striped morphologies without forming the nanopore structures at long treatment times. The morphological change in the Ar plasma-treated surface differs from that of the air plasma-treated surface, as can be seen in Figs. 9(i)−9(l). Even at a plasma treatment time of 2 s, stripe-like structures were generated together with a small number of grain-like structures on the treated surface regardless of the treatment time. Thus, the Ar

plasma treatment produced surface morphological changes even after a very short treatment time, but did not generate nanopore structures.

4. Discussion

Figures 6 and 7 demonstrate that the degrees of hydrophilicity induced by the air and Ar plasma jets correlated closely with the concentrations of oxygen-based FPGs grafted onto the sample surfaces. This correlation indicates that the hydrophilicity produced by the 3 l/min air plasma jet at a nozzle-to-sample distance of 1 mm after 1 min can be attributed to the larger amount of FPGs generated under these conditions. These new FPGs likely formed a hydrogen bond network with water molecules on the polymer surface [49,50], thus enhancing the hydrophilicity of the material after a brief treatment time. The larger number of oxygen-based FPGs grafted by the air plasma jet at the low gas flow rate and the low nozzle-to-sample distance after a short treatment time can be explained based on four key factors.

The first factor is the ability of the air plasma jet to impart a larger number of oxygen radical ions to the PP film surface. This is supported from the fact that the air plasma jet has the highest RMS I_S value at the low gas flow rate and the low nozzle-to-sample distance (Fig. 4). In general, O^- radical ions are generated in the air jet through the dissociative attachment of oxygen molecules due to the impact of electrons: $e + O_2 \rightarrow O^- + O$ [51,52], because air jet has 21% oxygen molecules. O_2^+ and O_3^- radical ions are also generated in the air jet through $e + O_2 \rightarrow O_2^+ + 2e$ and $O^- + O_2 \rightarrow O_3^-$ [51,52], and can decompose to oxygen atoms upon impacting with the surface [53]. In particular, the number of oxygen radical ions from the air plasma jet is considered to become the largest in the case of the highest RMS I_S value. Thus, these radical ions in the air plasma jet would imping on and react readily with carbon atoms on the PP film surfaces, increasing the number of oxygen-based FPGs [54,55].

The second factor is the ability of the air plasma to impart oxygen radicals to the PP film surface, i.e., the sticking of oxygen radicals to the surface. This is confirmed by the oxygen radical peak in the emission spectrum of the air plasma (Fig. 5). These radicals are generated through the dissociation of oxygen molecules in the air jet and in the ambient air due to the impact of electrons, via the reactions: $e + O_2 \rightarrow O + O^-$, $e + O_2 \rightarrow 2O + e$, and $e + O_2 \rightarrow O + O^+ + 2e$ [56,57]. These radicals are also generated through the dissociation of oxygen molecules due to the impact of vibrationally excited nitrogen molecules, as shown in Fig. 5, through the reaction $N_2 + O_2 \rightarrow O + O + N_2$ [36,58]. As a result, a large amount of oxygen radicals is present in the air plasma jet. These radicals would react with carbon atoms on the PP film surfaces more readily than oxygen molecules, thus forming a larger number of oxygen-based FPGs [54,55].

The third key factor is photo-oxidation [59−63] induced by UV photons emitted from the air plasma jet. The air plasma jet was found to generate photons with energies of 3.2−4.2 eV (see Fig. 5). Pure PP including no impurities does not absorb UV photons with energies less than approximately 6 eV, because it has an optical band-gap energy of approximately this value [63,64]. However, less energetic UV photons can be absorbed by residual impurities, such as chromophoric, carbonyl and hydroperoxy groups introduced during the fabrication process, traces of polymerization catalysts and charge transfer complexes formed between PP and oxygen [63]. Because the surface of the untreated PP film used in the present study was found to have 1% oxygen-based FPGs (Fig. 7), UV photons emitted from the air plasma jet could have been absorbed. This absorption would abstract hydrogen atoms from the surface CH_2=CH–CH_3 units to produce polymeric macro radicals or alkyl radicals, P· (such as CH=CH–CH_3 or CH_2=C–CH_3) [46−50]. These new species would react with oxygen radical ions and oxygen radicals from the air plasma jet impinging on the surface to a greater extent than with oxygen molecules, thus greatly increasing the amount of oxygen-based FPGs.

The fourth key factor is a thermal oxidation effect [65−69] induced by heat from the air plasma jet. Figure 10 summarizes the temporal changes in the temperatures of PP film surfaces treated with air and Ar plasma jets, based on remote measurements using a radiation thermometer (Horiba IT-545NH). In the case of the 3 l/min air plasma jet, the sample temperature increased to 51 °C as the treatment time was lengthened to 1 min. This value was higher than the 35 °C values for surfaces treated with 10 l/min air and 3 l/min Ar plasma jets. The higher temperature induced by the 3 l/min air plasma jet resulted from the conductive heating caused by the higher flux of charged plasma particles impinging on the sample (see Fig. 4). The higher sample temperature would be expected to facilitate hydrogen abstraction from the PP film surface to generate P· species [65−69], as in the case of UV-induced oxidation.

The morphological changes in the PP surfaces are also correlated with the concentrations of oxygen-based FPGs, as demonstrated by Figs. 7 and 9. This correlation confirms that the nanopore structures formed after 1 min exposure to the 3 l/min air plasma jet was related to the formation of a greater number of FPGs. These FPGs will cause extensive chain scission through chemical reactions at the PP film surface, thus emitting a larger quantity of volatile gases such as CO and CO_2 from the surface [59−63,65−69], which in turn may contribute to forming nanopore structures. Another effect that may contribute to the formation of nanopores is oxidation by UV photogenerated holes, as has been discussed in reports regarding GaN [70] and AlGaN [71] thin film surfaces treated with UV-assisted plasma. The optical band-gap energy of PP irradiated with energetic Ar^+ ions is reported to decrease to 2.8 eV as the energy of the Ar^+ ions increases to 50 keV [64]. This decrease is considered to be caused by the introduction of point defects and the formation of amorphous carbon [64]. Therefore, the present results suggest that photogenerated carriers can be produced in the damaged PP surface via the impact of photons with energies greater than 2.8 eV, rather than 6 eV.

When using the 3 l/min air plasma jet, charged plasma particles imparted to the surface may have introduced a large number of point defects and have generated amorphous carbon with the assistance of the above-discussed plasma-induced oxidation factors. These combined effects would be expected to decrease the optical band-gap energy of the PP film surface, such that holes were generated in the surface following the impact of photons with energies in the range of 3.2–4.2 eV. These UV photogenerated holes would promote extensive chain scission on the PP film surface through oxidative reactions, to produce volatile gases such as CH_2 and CH_3. This effect may also be responsible for the formation of nanopores on the surface.

In the case of Ar plasma jet treatment, there are the two key factors for increasing the number of the oxygen-based FPGs, i.e., the sticking of oxygen radicals and UV-induced oxidation which are considered to be greater than those induced by the air plasma jet (Fig. 5). However, the number of oxygen-based FPGs grafted by the Ar plasma jet is not large compared with the air plasma jet (Figs. 7 and 8). This suggests that the sticking of oxygen radicals and UV-induced oxidation do not contribute significantly to increasing the number of oxygen-based FPGs. Thus, the large number of oxygen-based FPGs produced by the air plasma jet can be attributed primarily to oxygen radical ions impinging from the air plasma jet on the surface. This can further be attributed secondarily to the heat-induced oxidation from the air plasma jet.

5. Conclusion

We have developed a new plasma jet device incorporating a twisted wires-cylindrical electrode configuration that generates an air-based nonequilibrium AP plasma jet. Using this device, we were able to clarify the effects of this plasma jet on the characteristics of PP film surfaces by comparing specimens treated with air- and Ar-based nonequilibrium AP plasma jets. The flux of charged particles imparted to the

sample surface by the air plasma jet was found to greatly increase with decreases in both the gas flow rate and nozzle-to-sample distance, in contrast to the results obtained using an Ar plasma jet. The hydrophilicity of a PP surface subjected to the air-based plasma jet was improved over a short treatment time of 1 min by reducing the gas flow rate and the nozzle-to-sample distance. This enhanced hydrophilicity can be attributed to the formation of a high concentration of oxygen-based FPGs containing C−O/C−OH and C=O/C=O−OH bonds on the polymer surface, such that 60% oxygen-based FPGs were obtained. The surface morphology associated with the enhanced hydrophilicity was found to be significantly different from those induced by other plasma jet conditions. Specifically, a large number of nanopores with diameters less than 1 μm were produced along a striped pattern. The large number of oxygen-based FPGs grafted during exposure to the air plasma jet over a short treatment time can be attributed primarily to oxygen radical ions impinging from the air plasma jet on the surface. This can further be attributed secondarily to the heat oxidation promoted by the plasma rather than the sticking of oxygen radicals and UV-induced oxidation from the plasma. The formation of nanopore structures can also be ascribed to oxidation from UV photogenerated holes.

Acknowledgements

We thank Edanz Group (www.edanzediting.com/ac) for editing a draft of this manuscript.

References

[1] Y. Zhang, J. J. Yuan, Y. Z. Song, X. Yin, C. C. Sun, L. P. Zhu, and B. K. Zhu, Tannic acid/polyethyleneimine-decorated polypropylene separators for Li-ion batteries and the role of the interfaces between separator and electrolyte, Electrochim. Acta **275** (2018) 25–31.

[2] T. Sato, H. Akiyama, S. Horiuchi, and T. Miyamae, Characterization of the polypropylene surface after atmospheric pressure N_2 plasma irradiation, Surf. Sci. **677** (2018) 93–98.

[3] S. Toommee and P. Pratumpong, PEG-template for surface modification of zeolite: a convenient material to the design of polypropylene based composite for packaging films, Results Phys. **9** (2018) 71–77.

[4] H. Jmal, N. Bahloli, C. W. Kocher, D. Leray, F. Ruch, J. N. Munsch, and M. Nardin, Influence of the grade on the variability of the mechanical properties of polypropylene waste, Waste Manage. **75** (2018) 160–173.

[5] A. Rosehr, D. Griebe, and G. A. Luinstra, Graphite nanosheets - polypropylene composites from in toluene delaminated graphite using atactic polypropylene as dispersant, Compos. Sci. Technol. **156** (2018) 28–38.

[6] M. S. Curcio, M. C. Canela, and W. R. Waldman, Selective surface modification of TiO_2-coated polypropylene by photodegradation, Eur. Polym. J. **101** (2018) 177–182.

[7] C. Zhang, Y. Bai, B. Cheng, and W. Liu, Adhesion properties of atactic polypropylene/acrylate blend copolymer and its adhesion mechanism for untreated polypropylene materials, Int. J. Adhes. Adhes. **80** (2018) 7–15.

[8] H. R. Ghorbani and M. Molaei, Antibacterial nanocomposite preparation of polypropylene-silver using corona discharge, Prog. Org. Coat. **112** (2017) 187–190.

[9] G. Acik, G. Altinkok, H. Olmez, and M. A. Tasdelen, Antibacterial film from chlorinated polypropylene via CuAAC click chemistry, Prog. Org. Coat. **125** (2018) 73–

78.

[10] S. Kalnaus, Y. Wang, J. Li, A. Kumar, and J. A. Turner, Temperature and strain rate dependent behavior of polymer separator for Li-ion batteries, Extreme Mech. Lett. **20** (2018) 73–80.

[11] W. Brostow, I. K. Chen, N. Hnatchuk, J. Hrbacek, A. Hull, R. H. Pahler, and A. Srinivasan, Enhanced adhesion of polypropylene to copper substrates, Polym. Test. **63** (2017) 158–162.

[12] X. Li, N. Gong, C. Yang, S. Zeng, S. Fu, and K. Zhang, Aluminum/polypropylene composites produced through injection molding, J. Mater. Process. Technol. **255** (2018) 635–643.

[13] W. M. Gao, L. Wang, J. K. Coffey, and F. Daver, Finite element simulation of scratch on polypropylene panels, Mater. Des. **140** (2018) 400–408.

[14] H. J. Jeon and M. N. Kim, Isolation of mesophilic bacterium for biodegradation of polypropylene, Int. Biodeterior. Biodegrad. **115** (2016) 244–249.

[15] D. Pulungan, A. Yudhanto, S. Goutham, G. Lubineau, R. Yaldiz, and W. Schijve, Characterizing and modeling the pressure- and rate-dependent elastic-plastic-damage behavior of polypropylene-based polymers, Polym. Test. **68** (2018) 433–445.

[16] X. Zhu, X. Shi, Z. Pan, Y. Fang, and Y. Wu, Photo-grafting polymerization, microstructure and hydrophilicity of spun-blown polypropylene nonwoven fabrics, IOP Conf. Series: Mater. Sci. Eng. **254** (2017) 122014:1–6.

[17] A. R. Oromiehie, H. E. Dehaghani, K. Ansari, K. Karimi, Z. Rahmani, and S. Mirbagheri, Preparation and characterization of functionalized polypropylene with acrylamide and itaconic acid, J. Mater. Sci. Chem. Eng. **2** (2014) 43–51.

[18] A. Sarani, N. D. Geyter, A. Y. Nikiforov, R. Morent, C. Leys, J. Hubert, and F. Reniers, Surface modification of PTFE using an atmospheric pressure plasma jet in argon and argon + CO_2, Suf. Coat. Tech. **206** (2012) 2226–2232.

[19] P. Terebun, M. Kwiatkowski, P. Mazurek, and J. Pawlat, Impact of radio frequency atmospheric-pressure plasma on water contact angles of high-impact polystyrene, Sens. Mater. **30** (2018) 1213–1220.

[20] J. I. Podsiadly and E. Dorsam, Effects of argon flow temperature plasma on PLA film surface and aging behavior, Vacuum **145** (2017) 278−284.

[21] T. S. M. Mui, R. P. Mota, A. Quade, L. R. O. Hein, and K. G. Kostov, Uniform surface modification of polyethylene terephthalate (PET) by atmospheric pressure plasma jet with a horn-like nozzle, Suf. Coat. Tech. **352** (2018) 338–347.

[22] Y. Takemura, N. Yamaguchi, and T. Hara, Study on surface modification of polymer Films by using atmospheric plasma jet source, Jpn. J. Appl. Phys. **47** (2008) 5644–5647.

[23] J. Choi, K. Matsuo, H. Yoshida, T. Namihira, S. Katsuki, and H. Akiyama, Characteristics of a dc-driven atmospheric pressure air microplasma jet, Jpn. J. Appl. Phys. **47** (2008) 6459–6463.

[24] F. Fanelli and F. Fracassi, Atmospheric pressure non-equilibrium plasma jet technology: general features, specificities and applications in surface processing of materials, Surf. Coat. Technol. **322** (2017) 174–201.

[25] T. M. C. Nishime, A. C. Borges, C. Y. K. Ito, M. Machida, L. R. O. Hein, and K. G. Kostov, Non-thermal atmospheric pressure plasma jet applied to inactivation of different microorganisms, Surf. Coat. Technol. **312** (2017) 19–24.

[26] D. P. Dowling, F. T. Oneil, S. J. Langlais, and V. J. Law, Influence of dc pulsed atmospheric pressure plasma jet processing conditions on polymer activation, Plasma Process. Polym. **8** (2011) 718–727.

[27] M. Kwiatkowski, P. Terebun, P. Mazurek, and J. Pawlat, Wettability of polymeric materials after dielectric barrier discharge atmospheric-pressure plasma jet treatment, Sens. Mater. **30** (2018) 1207–1212.

[28] A. Sarani, A. Y. Nikiforov, N. D. Geyter, R. Morent, and C. Leys, Surface modification of polypropylene with an atmospheric pressure plasma jet sustained in argon and an argon/water vapor mixture, Appl. Surf. Sci. **257** (2011) 8737–8741.

[29] F. Rombaldoni, K. Mahmood, A. Varesano, M. B. Songia, A. Aluigi, C. Vineis, and G. Mazzuchetti, Adhesion enhancement of electrospun nanofiber mats to polypropylene nonwoven fabric by low-temperature oxygen plasma treatment, Suf. Coat. Tech. **216** (2013) 178–184.

[30] W. X. Chen, J. S. Yu, W. Hu, and G. L. Chen, Partial hydrophilic modification of biaxially oriented polypropylene film by an atmospheric pressure plasma jet with the allylamine monomer, Appl. Surf. Sci. **387** (2016) 957–964.

[31] M. Grushin, N. Dyatko, I. Kochetov, A. Napartovich, N. Trushkin, T. M. Duc, and S. Descours, Studies on cold plasma–polymer surface interaction by example of PP- and PET-films, J. Phys. D: Appl. Phys. **41** (2008) 235203:1−13.

[32] T. Jacobs, E. Carbone, R. Morent, N. D. Geyter, F. Reniersb, and C. Leysa, Surface modification of polymer films with a remote atmospheric pressure d.c. glow discharge: influence of substrate location, Sur. Interface Anal. **42** (2010) 1316−1320.

[33] A. H. Basher and A. H. Mohamed, Laminar and turbulent flow modes of cold atmospheric pressure argon plasma jet, J. Appl. Phys. **123** (2018) 193302:1−9.

[34] S. Nunomura, M. Kondo, and H. Akatsuka, Gas temperature and surface heating in plasma enhanced chemical-vapour-deposition, Plasma Sources Sci. Technol. **15** (2006) 783−789.

[35] H. S. Uhm, S. J. Jung, and H. S. Kim, Influence of gas temperature on electrical breakdown in cylindrical electrodes, J. Korean Phys. Soc. **42** (2003) S989−S993.

[36] X. L. Deng, A. Y. Nikiforov, P. Vanraes, and C. Leys, Direct current plasma jet at atmospheric pressure operating in nitrogen and air, J. Appl. Phys. **113** (2013) 023305:1–9.

[37] P. Paris, M. Aints, F. Valk, T. Plank, A. Haljaste, K. V. Kozlov, and H. E. Wagner, Intensity ratio of spectral bands of nitrogen as a measure of electric field strength in plasmas, J. Phys. D: Appl. Phys. **38** (2005) 3894–3899.

[38] L. Cong, Z. Jialiang, Y. Zhi, W. Xingwei, Z. Chenfei, and D. Hongbin, Diagnosis of Electron, vibrational and rotational temperatures in an Ar/N_2 shock plasma jet produced by a low pressure DC cascade arc discharge, Plasma Sci. Technol. **15** (2013) 875–880.

[39] J. J. Camacho, J. M. L. Poyato, L. Diaz, and M. Santos, Optical emission studies of nitrogen plasma generated by IR CO_2 laser pulses, J. Phys. B: At. Mol. Opt. Phys. **40** (2007) 4573–4590.

[40] C. Biloiu, X. Sun, Z. Harvey, and E. Scimen, An alternative method for gas temperature determination in nitrogen plasmas: fits of the bands of the first positive system ($B^3\Pi_g \rightarrow A^3\sum_u^+$), J. Appl. Phys. **101** (2007) 073303:1–11.

[41] R. C. Boutwell, M. Wei, M. Baudelet, and W. V. Schoenfeld, Investigation and impact of oxygen plasma compositions on cubic ZnMgO grown by molecular beam epitaxy, J. Alloy Compd. **584** (2014) 327–330.

[42] NIST Atomic Spectra Database, https://www.nist.gov/pml/atomic-spectra-database.

[43] X. Li, X. Lin, K. Wu, C. Ren, R. Liu, and P. Jia, Regularly-swelling plumes generated in atmospheric pressure argon plasma jet excited by a biased sinusoidal voltage, Plasma Sources Sci. Technol. **28** (2019) 055006:1−7.

[44] A. Sarani, A. Y. Nikiorov, and C. Leys, Atmospheric pressure plasma jet in Ar and Ar/H_2O mixtures: optical emission spectroscopy and temperature measurements, Phys. Plasmas **17** (2010) 063504:1−8.

[45] R. Morent, N. G. Geyter, C. Leys, L. Gengembre, and E. Payen, Comparison between XPS- and FTIR-analysis of plasma-treated polypropylene film surfaces, Surf. Interface Anal. **40** (2008) 597–600.

[46] K. G. Kostov, T. M. C. Nishime, A. H. R. Castro, A. Toth, and L. R. O. Hein, Surface modification of polymeric materials by cold atmospheric plasma jet, Appl. Surf. Sci. **314** (2014) 367–375.

[47] G. P. Lopez, D. G. Castner, and B. D. Ratner, XPS O 1s binding energies for polymers containing hydroxyl, ether, ketone and ester groups, Surf. Interface Anal. **17** (1991) 267-272.

[48] N. Stribeck, A. Zeinolebadi, M. G. Sari, S. Botta, K. Jankova, S. Hvilsted, A. Drozdov, R. Klitkou, C. G. Potarniche, J. C. Chirstiansen, and V. Ermini, Properties and semicrystalline structure evolution of polypropylene/montmorillonite nanocomposites under mechanical load, Macromolecules **45** (2012) 962–973.

[49] L. Huang, K. E. Gubbins, L. Li, and X. Lu, Water on titanium dioxide surface: a revisiting by reactive molecular dynamics simulations, Langmuir **30** (2014) 14832–14840.

[50] P. Gilormini and J. Verdu, On the role of hydrogen bonding on water absorption in polymers, Polymer **142** (2018) 164–169.

[51] A. Yang, M. Rong, X. Wang, D. Liu, and M. G. Kong, Variable radio-frequency cold atmospheric He + O_2 discharges: from electron-heating mechanism to reactive species delivery, J. Phys. D: Appl. Phys. **46** (2013) 415201:1–14.

[52] S. Dahle, R. Gustus, W. Viöl, and W. M. Friedrichs, DBD Plasma Treatment of Titanium in O_2, N_2 and Air, Plasma Chem. Plasma Process. **32** (2012) 1109–1125.

[53] C. Morant, L. Galan, and J. M. Sanz, X-ray photoelectron spectroscopic study of the oxidation of polycrystalline rhenium by exposure to O_2 and low energy O_2^+ ions, Anal. Chim. Acta **297** (1994) 179–186.

[54] M. Golda, M. B. Wloch, M. Faryna, K. Engvall, and A. Kotarba, Oxygen plasma functionalization of parylene C coating for implants surface: nanotopography and active sites for drug anchoring, Mater. Sci. Eng. C **33** (2013) 4221–4227.

[55] J. Zhu, H. Deng, W. Xue, and Q. Wang, Effect of low temperature oxygen plasma treatment on microstructure and adhesion force of graphene, Appl. Surf. Sci. **428** (2018) 941–947.

[56] J. T. Gudmundsson, I. G. Kouznetsov, K. K. Patel, and M. A. Lieberman, Electronegativity of low-pressure high-density oxygen discharges, J. Phys. D: Appl. Phys. **34** (2001) 1100–1109.

[57] M. Imaru, N. U. Rehman, A. W. Khan, M. Z. Islam, M. Shafiq, and M. Zakaullah, Spectroscopic study of 50 Hz pulsed Ar–O_2 mixture plasma, Radiat. Phys. Chem. **123** (2016) 115–121.

[58] H. Yoshiki, Generation of air microplasma jet and its application to local etching of polyimide films, Jpn. J. Appl. Phys. **45** (2006) 5618–5623.

[59] M. C. Mistretta, L. Botta, A. D. Vinci, M. Ceraulo, and F. P. L. Mantia, Photo-oxidation of polypropylene/graphene nanoplatelets composites, Polym. Degrad. Stabil. **160** (2019) 35–43.

[60] E. Yousif and R. Haddad, Photodegradation and photostabilization of polymers, especially polystyrene: review, SpringerPlus **2** (2013) 398:1–32.

[61] J. Zhao, R. Yang, and J. Yu, Interfacial effect on photo-oxidation of PP via model blends, Polym. Degrad. Stabil. **98** (2013) 1981–1987.

[62] J. F. Larche, P. O. Bussiere, S. Therias, and J. L. Gardette, Photooxidation of polymers: relating material properties to chemical changes, Polym. Degrad. Stabil. **97** (2012) 25–34.

[63] S. Aslanzadeh and M. H. Kish, Photo-oxidation of polypropylene fibers exposed to short wavelength UV radiations, Fiber Polym. **11** (2010) 710–718.

[64] S. F. Ahmed, M. W. Moon, C. Kim, Y. J. Jang, S. Han, J. Y. Choi, W. W. Park, and K. R. Lee, Optical properties of surface modified polypropylene by plasma immersion ion implantation technique, Appl. Phys. Lett. **97** (2010) 081908:1–3.

[65] X. Li, J. Wang, Y. Sun, D. Zhang, N. Zhu, and L. Jing, The effect of thermal treatment on the decomposition of phthalonitrile polymer and phthalonitrile-polyhedral oligomeric silsesquioxane (POSS) copolymer, Polym. Degrad. Stabil. **156** (2018) 279–291.

[66] L. Chen, S. Yamane, T. Sago, H. Hagihara, S. Kutsuna, T. Uchimaru, H. Suda, H. Sato, and J. Mizukado, Experimental and modeling approaches for the formation of hydroperoxide during the auto-oxidation of polymers: thermal-oxidative degradation of polyethylene oxide, Chem. Phys. Lett. **657** (2016) 83–89.

[67] Y. Lv, Y. Huang, M. Kong, and G. Li, Improved thermal oxidation stability of polypropylene films in the presence of β-nucleating agent, Polym. Test. **32** (2013) 179–186.

[68] T. Seguchi, K. Tamura, A. Shimada, M. Sugimoto, and H. Kudoh, Mechanism of antioxidant interaction on polymer oxidation by thermal and radiation ageing, Radiat. Phys. Chem. **81** (2012) 1747–1751.

[69] G. Grynova, J. L. Hodgson, and M. L. Coote, Revising the mechanism of polymer autooxidation, Org. Biomol. Chem. **9** (2011) 480–490.

[70] R. Kawakami, M. Niibe, Y. Nakano, T. Shirahama, K. Aoki, K. Oba, M. Takabatake, and T. Mukai, Damage characteristics of n-GaN thin film surfaces etched by ultraviolet light-assisted helium plasmas, Thin Solid Films **570** (2014) 81–86.

[71] R. Kawakami, M. Niibe, Y. Nakano, and T. Mukai, AlGaN surfaces etched by CF_4 plasma with and without the assistance of near-ultraviolet irradiation, Vacuum **136** (2017) 28–35.

Figure captions:

Fig. 1. Schematic drawing of air plasma jet device consisting of a twisted wires-cylinder electrode configuration.

Fig. 2. Photographs of (a) the setup before discharge, (b) air plasma jet discharge, and (c) Ar plasma jet discharge.

Fig. 3. (a) Waveform of the voltage applied to the twisted wires and (b)−(e) waveforms of discharge currents following into the cylinder electrode and the sample stage, I_C and I_S, for 3 and 10 l/min air plasma jets at a nozzle-to-sample distance of 1 mm.

Fig. 4. RMS discharge currents flowing into the cylinder electrode and the sample stage, I_C and I_S, for air and Ar plasma jets generated at various nozzle-to-sample distances, as a function of gas flow rate.

Fig. 5. Comparison between the spectra of light emitted from (a) air and (b) Ar plasma jets. The inset shows the Ar plasma spectrum magnified at the UV range of 280−400 nm in wavelength.

Fig. 6. Contact angles of PP film surfaces treated with air and Ar plasma jets, as a function of treatment time. In each figure, the contact angle at zero treatment time corresponds to that of untreated PP film surface.

Fig. 7. XPS spectra of C 1s regions of (a) untreated PP film surface, (b) 3 l/min air plasma-treated surface, (c) 10 l/min air plasma-treated surface, and (d) 3 l/min Ar

plasma-treated surface, at a treatment time of 1 min and a nozzle-to-sample distance of 1 mm. (e) Comparison between chemical compositions of the plasma-treated surfaces.

Fig. 8. XPS spectra of O 1s regions of (a) 3 l/min air plasma-treated surface, (b) 10 l/min air plasma-treated surface, and (c) 3 l/min Ar plasma-treated surface, at a nozzle-to-sample distance of 1 mm. (d) Comparison between the ratios of O=C to O−C of the plasma-treated surfaces.

Fig. 9. SEM images of PP film surfaces treated with 3 and 10 l/min air plasma jets and with 3 l/min Ar plasma jet at a nozzle-to-sample distance of 1 mm.

Fig. 10. Temperatures of PP film surfaces treated with air and Ar plasma jets, as a function of treatment time.

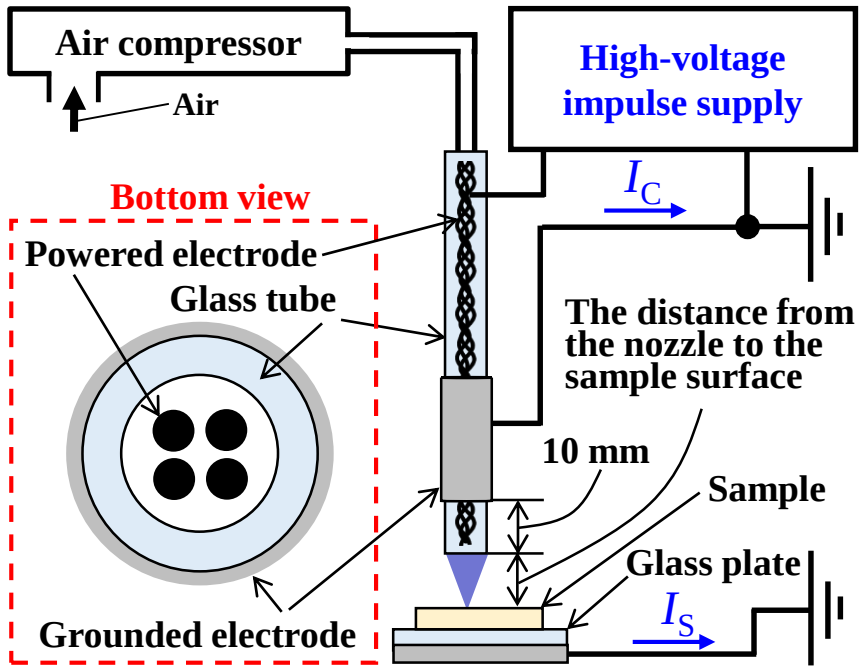

Fig. 1. R. Kawakami *et al.*

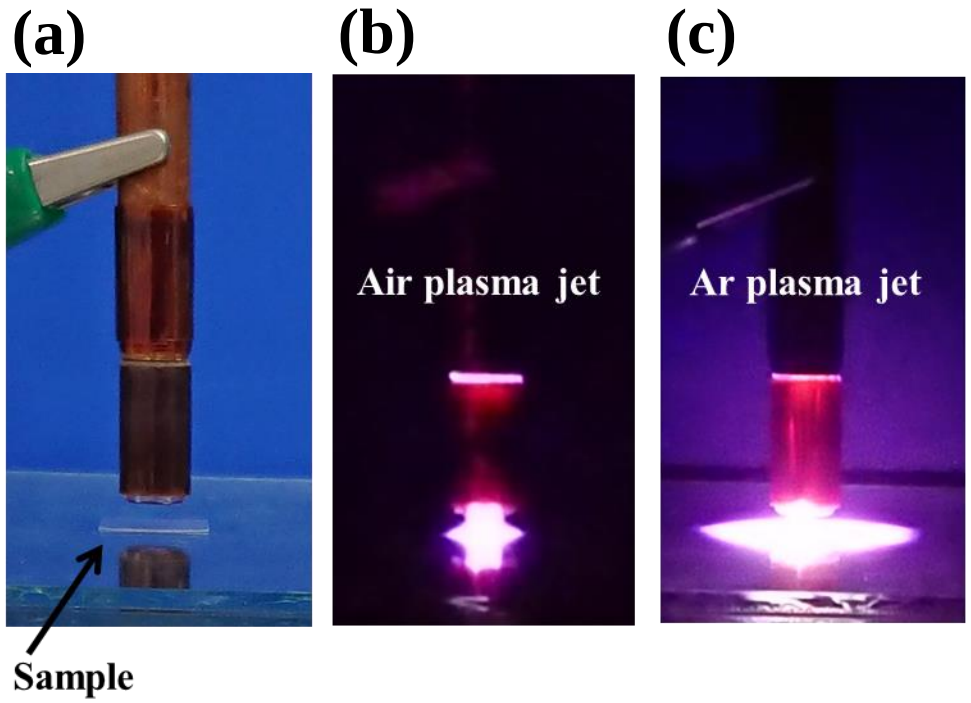

Fig. 2. R. Kawakami *et al.*

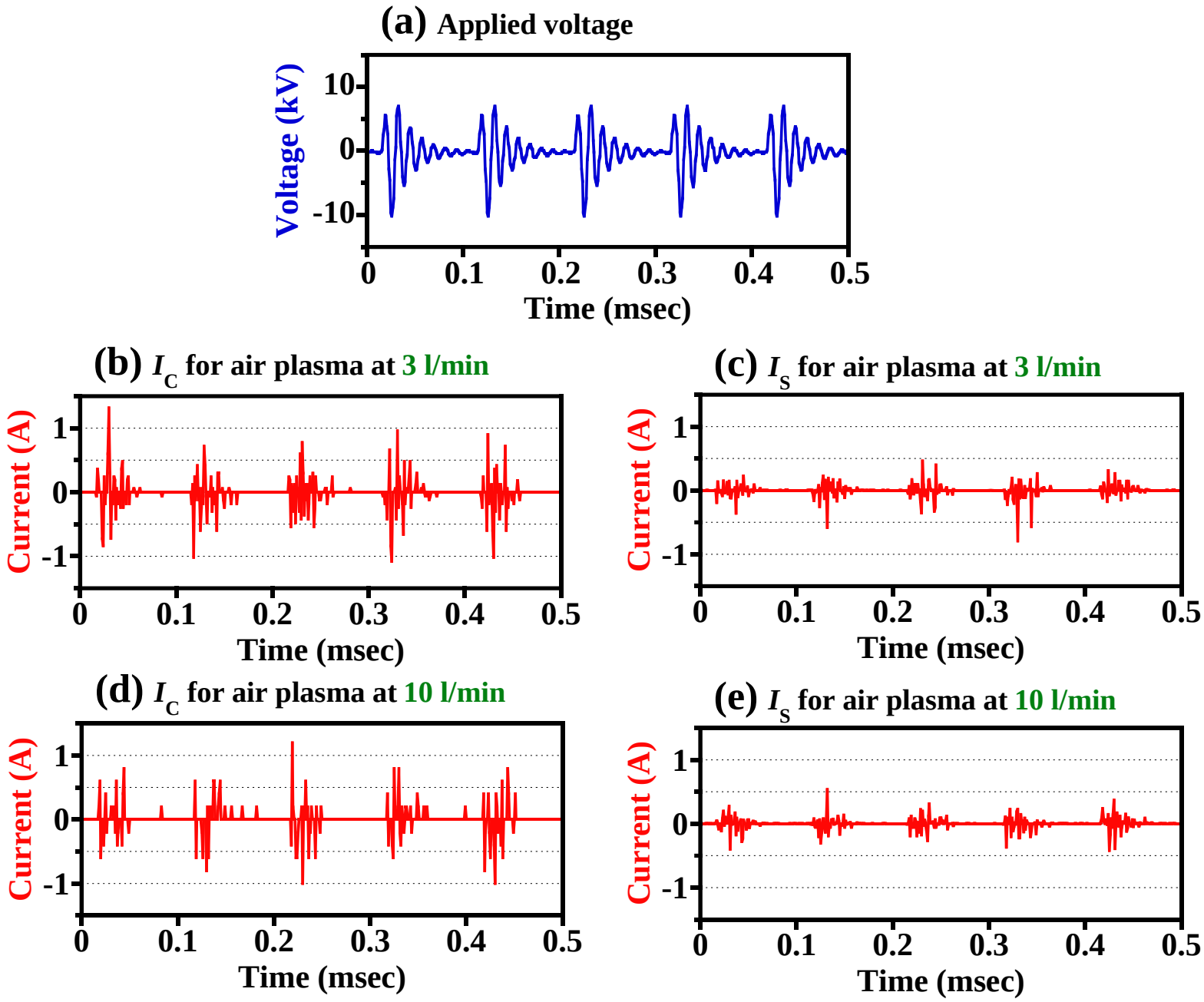

Fig. 3. R. Kawakami *et al.*

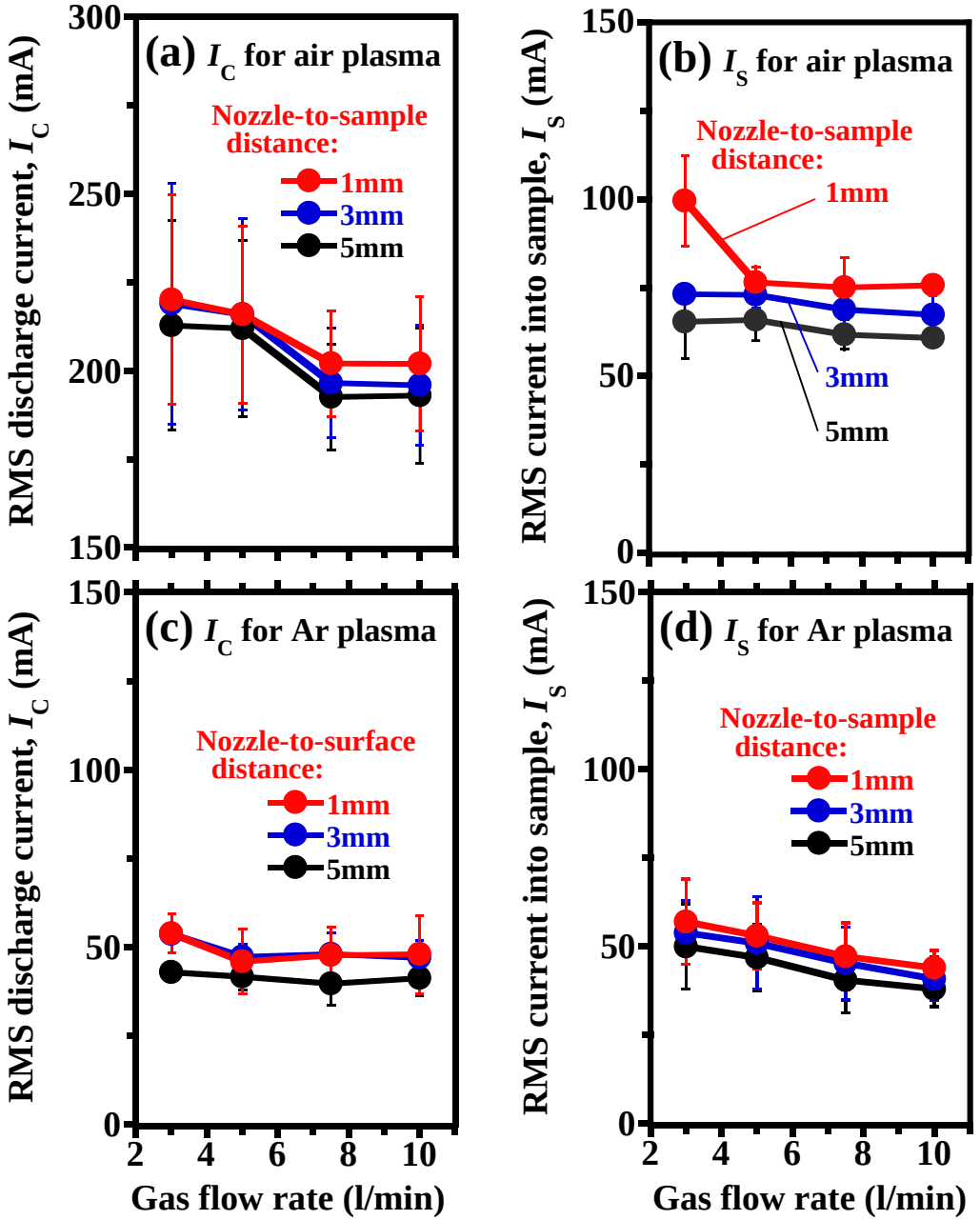

Fig. 4. R. Kawakami *et al.*

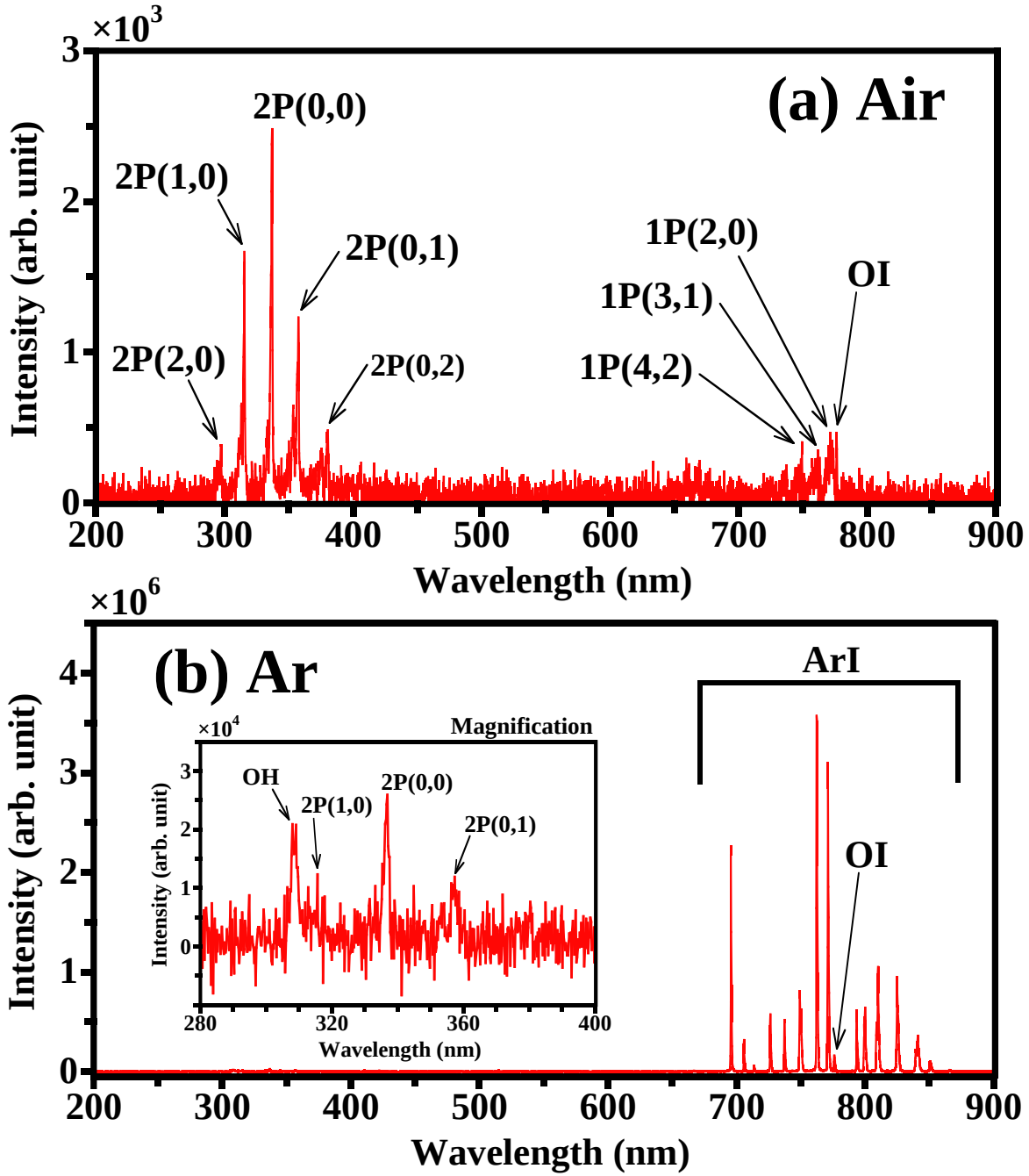

Fig. 5. R. Kawakami *et al.*

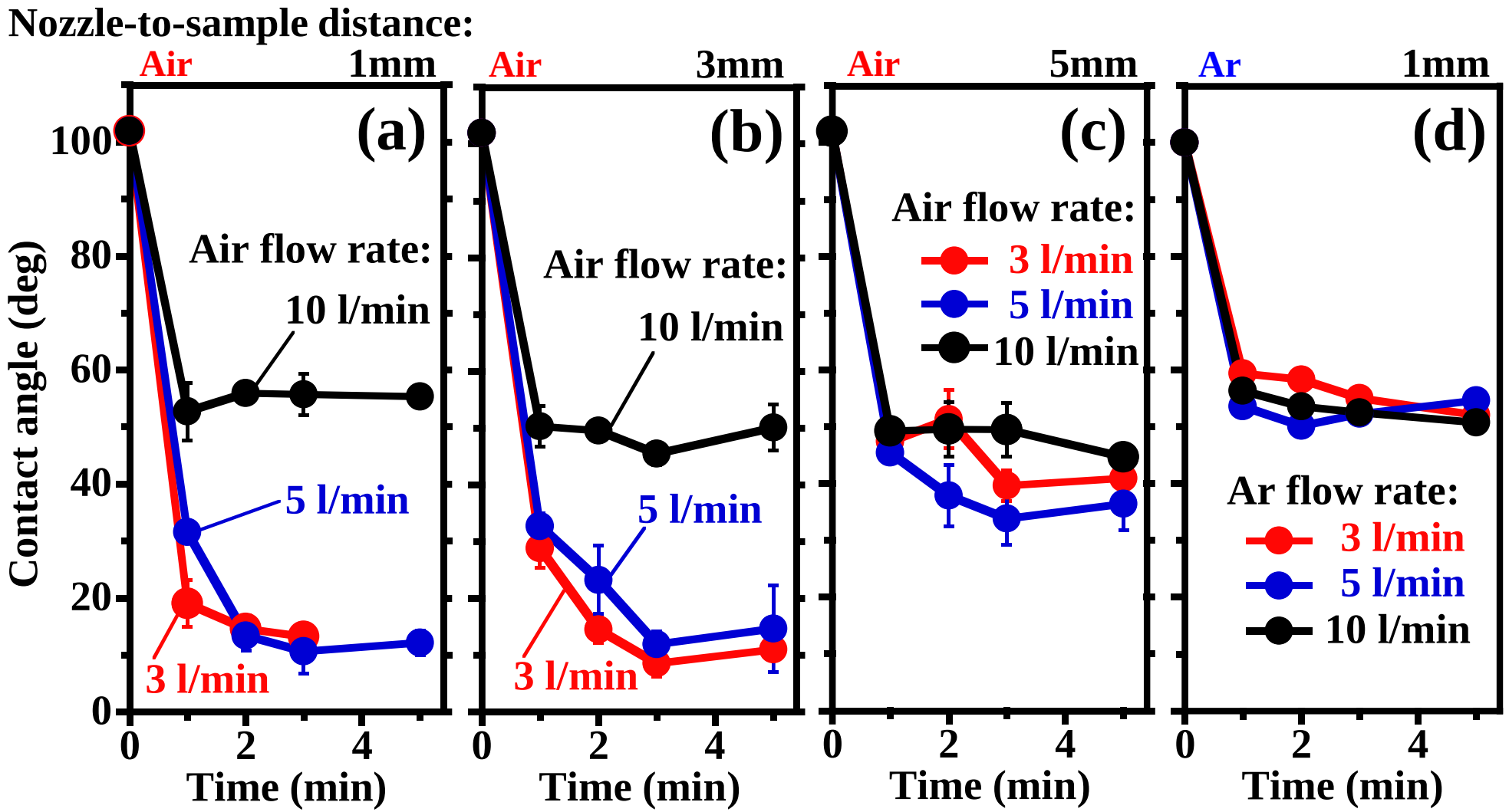

Fig. 6. R. Kawakami *et al.*

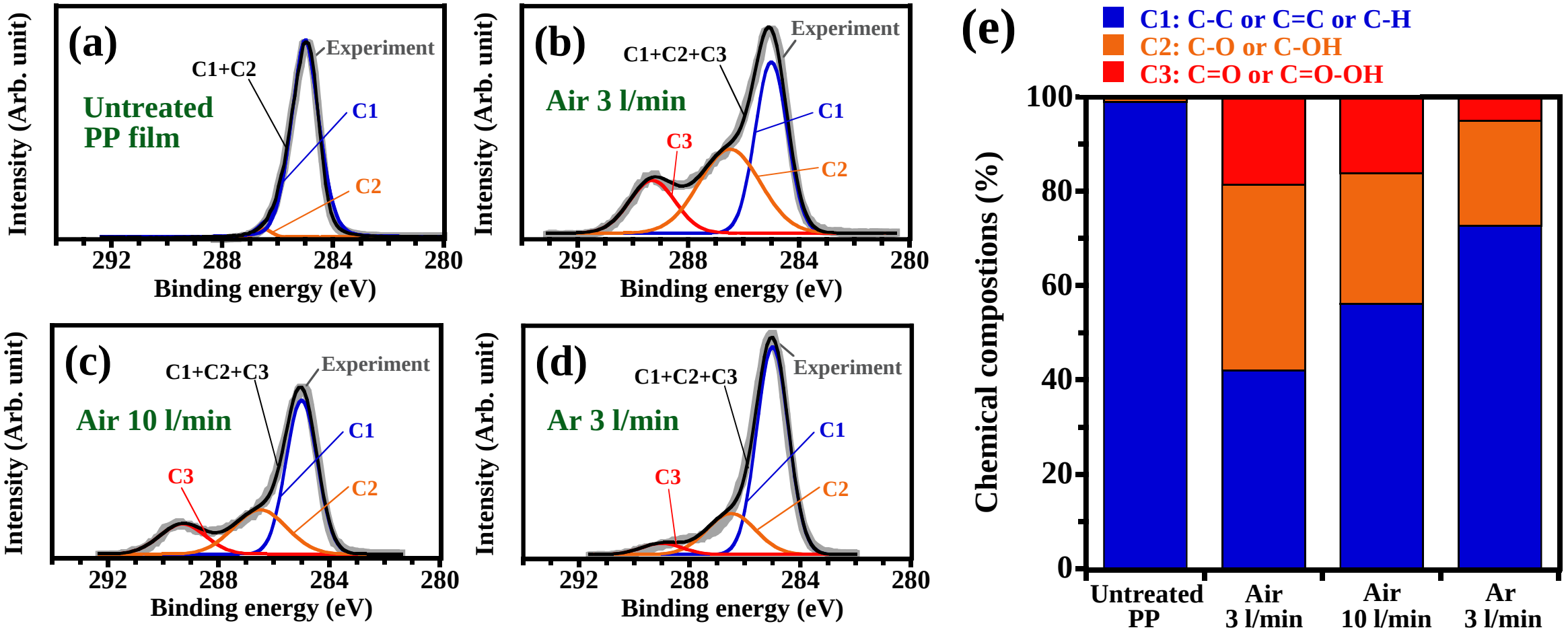

Fig. 7. R. Kawakami *et al.*

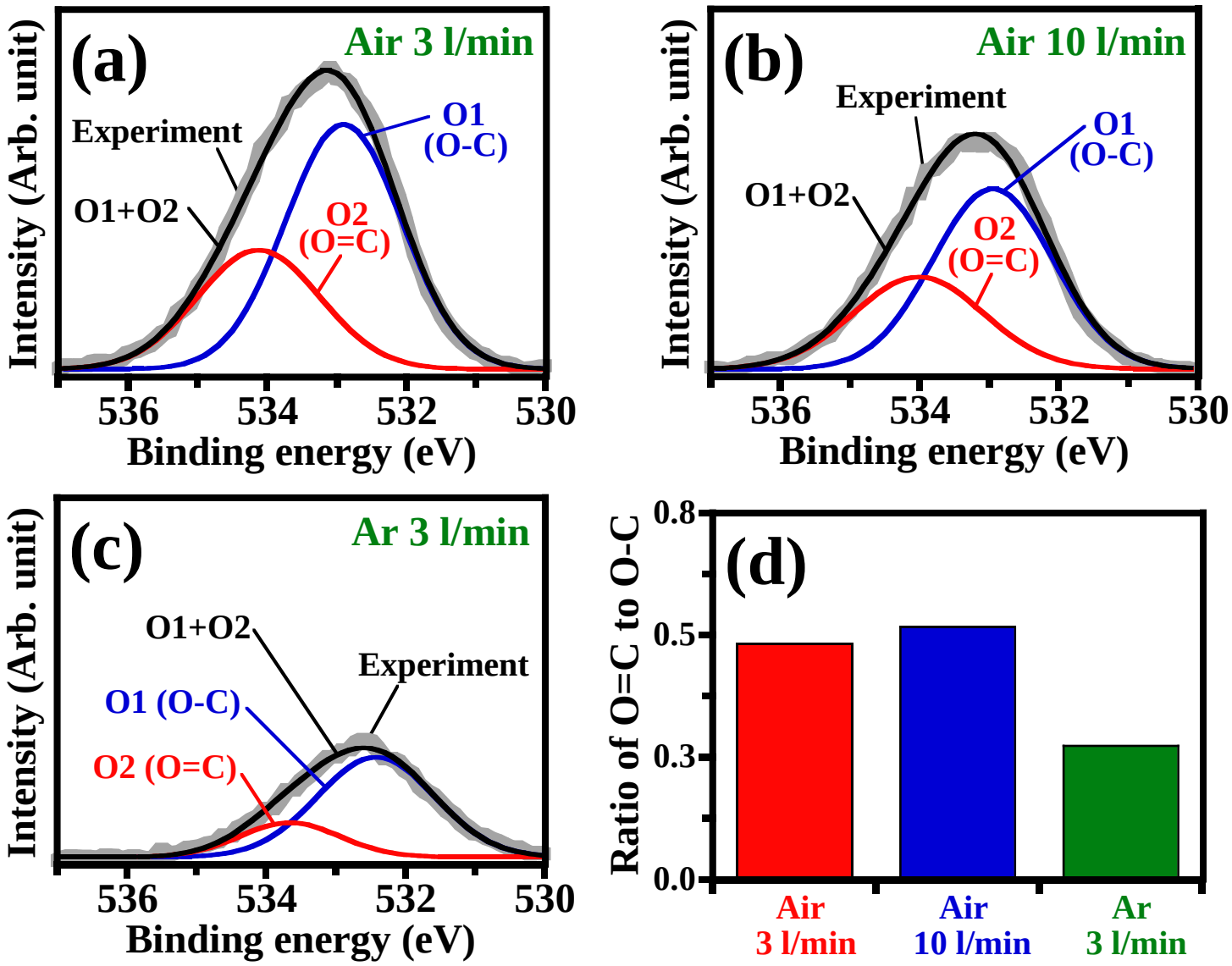

Fig. 8. R. Kawakami *et al.*

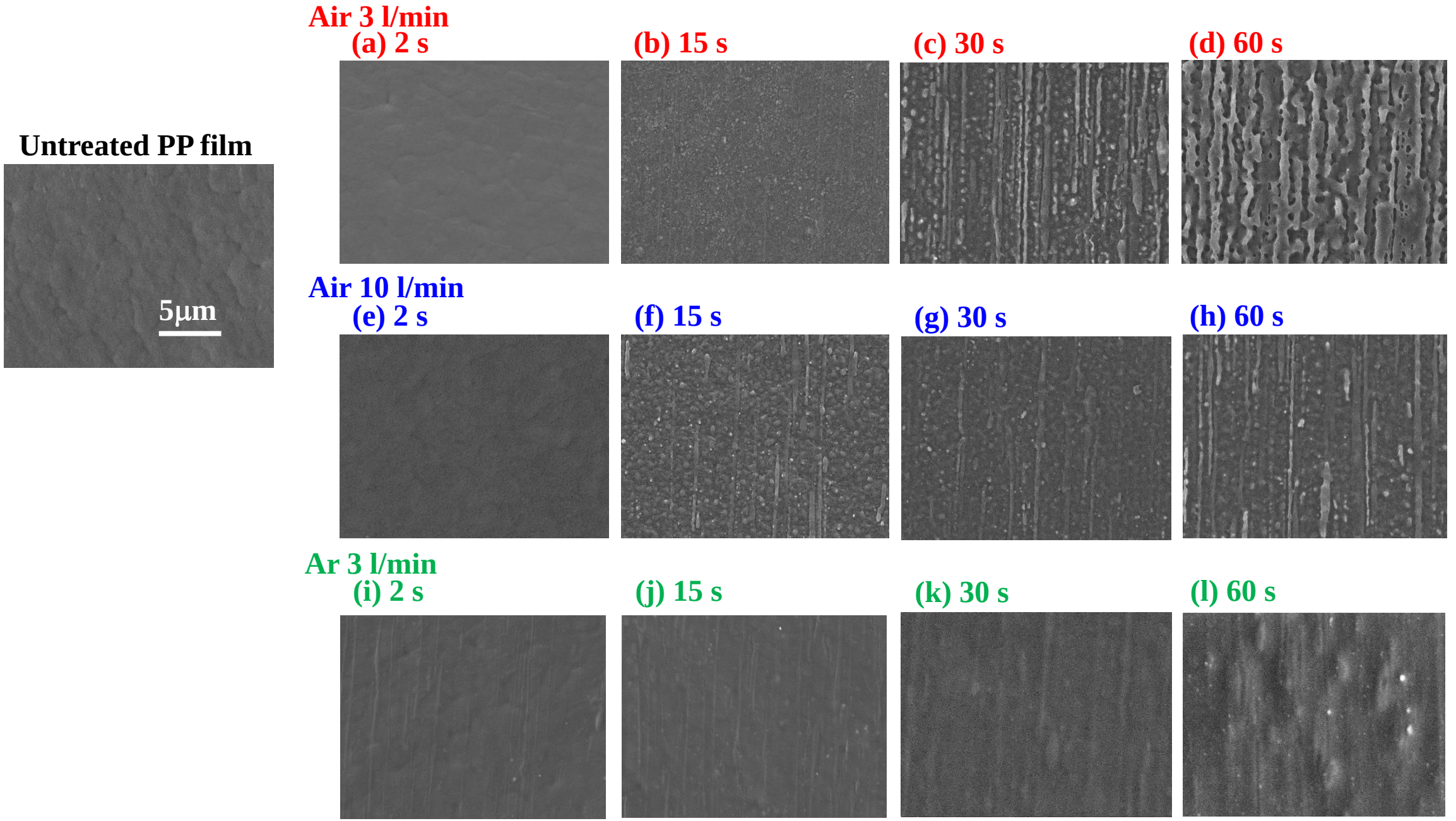

Fig. 9. R. Kawakami *et al.*

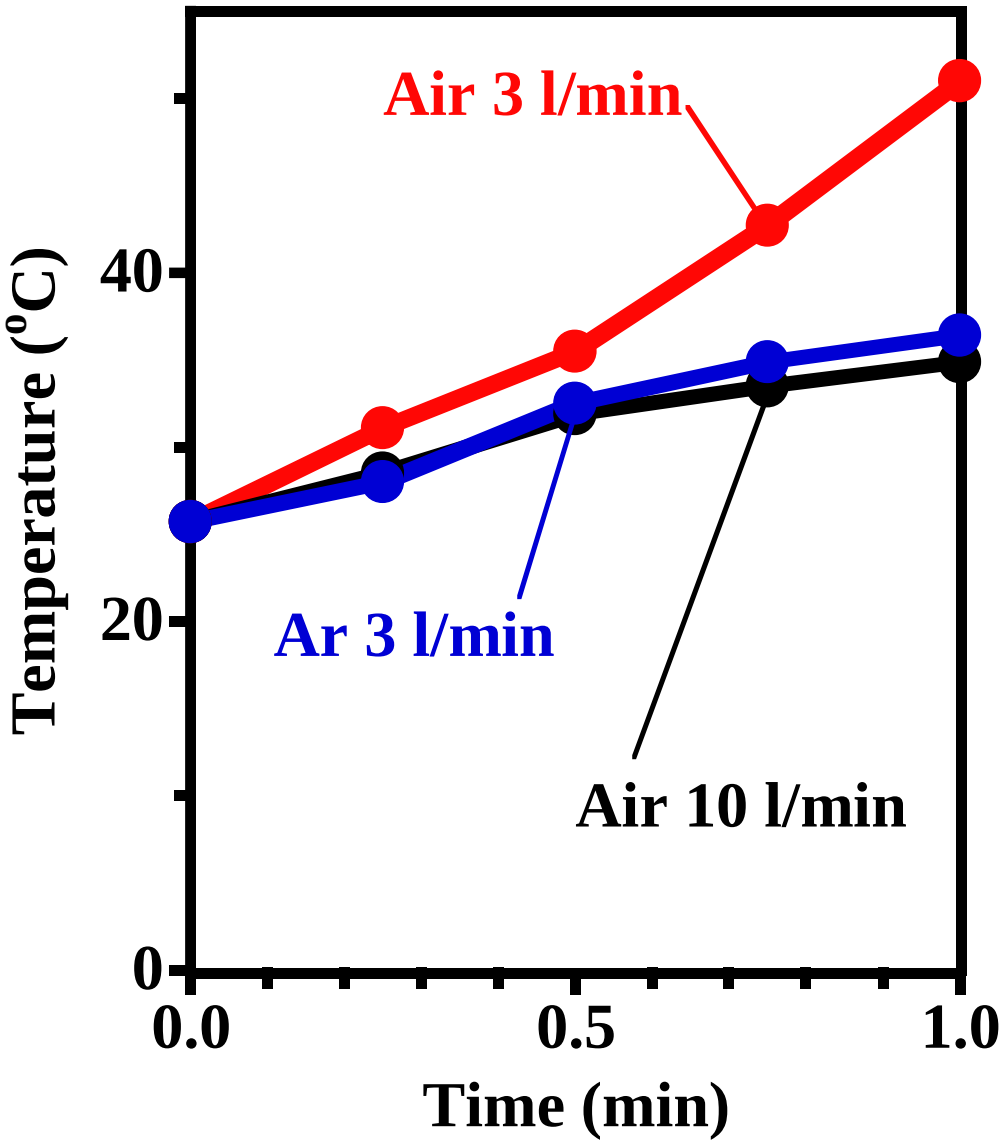

Fig. 10. R. Kawakami *et al.*